Catalytic Decomposition of N_2O on CaO and MgO: Experiments and ab Initio Calculations

Anders Snis* and Heije Miettinen

Department of Inorganic Chemistry, Göteborg University, S-412 96 Göteborg, Sweden

Received: November 5, 1997

Experiments and ab initio calculations have been performed to study the catalytic activity of calcium oxide and magnesium oxide toward N_2O decomposition. The experiments were carried out in a fixed-bed quartz reactor in the temperature range 773−1223 K. The decomposition of N_2O appeared to be a first-order reaction with activation energies of 26 kcal/mol for CaO and 36 kcal/mol for MgO, respectively. The decomposition rate did not change when excess oxygen was introduced to the inlet gas. The ab initio energy barriers of the dissociative reaction: $N_2O(g) + O^{2-}_{surf} \rightarrow N_2(g) + O^{2-}_{2,surf}$, in which the oxygen anion is seated in a CaO(100) or MgO(100) model surface, are 22 and 33 kcal/mol. High-temperature preexponential factors and activation energies are estimated from transition-state theory and collision theory expressions. The values agree well with those obtained experimentally. This indicates that most of the surface anions of both CaO and MgO are active in decomposing N_2O in the temperature range investigated. A model of a plug-flow reactor is used to demonstrate that the temperature dependence of the overall reaction rate obtained at high N_2O concentrations reflects the regenerating process of the surface and not the molecular dissociation of N_2O.

1. Introduction

The catalytic activity and the basicity of calcium and magnesium oxides have been investigated in several works. Both experimental and computational efforts are reported. In a theoretical work Pacchioni et al. studied the chemisorption of CO_2 and SO_2 on CaO(100) and MgO(100) surfaces by ab initio cluster calculations.[1] Both molecules formed rather strong chemisorbed complexes with an oxygen anion seated in the CaO(100) surface, whereas only weak bonds were obtained for the MgO(100) surface. The higher activity of CaO was explained by its larger cation, which results in a larger lattice constant for CaO than for MgO, 2.4 Å compared to 2.1 Å. As a consequence, the Madelung potential that a surface oxygen ion experiences is lower for calcium oxide, and the energy cost to use the charge of $O^{2-}_{CaO(100)}$ ions in chemical bonds is lower. A similar argument was used by Nygren and Pettersson to explain the weaker oxygen bond in the surface peroxide species, $O^{2-}_{2,MgO(100)}$, compared to that of $O^{2-}_{2,CaO(100)}$.[2] The difference in basicity is thus established to be of electrostatic nature and the accompanying chemical activity is expected to increase along the series MgO < CaO < SrO < BaO.[1] Accordingly, it is not surprising to find CaO more efficient in decomposing N_2O than MgO.[3,4] However, it is not clear to what extent five-coordinated O^{2-}_{100} ions in the MgO surface participate in the dissociative reaction of N_2O.[2]

The O^{2-}_{100} ions are assumed to be the predominant anions in the surfaces of basic oxides such as CaO and MgO, and for CaO they are expected to be active in the decomposition of N_2O. This was demonstrated by Nakamura et al., who used infrared (IR) spectroscopy to characterize the adsorbed species formed on a CaO surface exposed to N_2O.[5] The IR frequency of 880 cm^{-1} obtained corresponds well to a peroxy-type bond. A similar ab initio vibrational frequency was achieved for an O_2^{2-} ion seated in a CaO(100) model surface.[6] Nakamura et al. also performed temperature-programmed desorption (TPD) experiments to study the amount of oxygen species adsorbed. The maximum coverage was approximately 0.5, and the oxygen desorption occurred at 643−740 K.

The activation energy for decomposing N_2O on CaO was determined by Winter to be 34 kcal/mol in the temperature range 443−653 K.[4] On limestone the activation energy is 22−23 kcal/mol in the temperature range 770−1100 K.[7,8] The difference might to some extent be explained by small amounts of impurities present in the limestone, whereas Winter used a more pure substrate. However, the temperature used in the latter work is below the oxygen desorption temperature of Nakamura. This combined with the high N_2O concentration used (10−26%) suggests that the activity obtained by Winter was influenced by the adsorbed oxygen species.

In a previous ab initio computational work[9] a mechanism for the dissociative reaction

$$N_2O + O^{2-}_{CaO} \rightarrow N_2 + O^{2-}_{2,CaO}$$

was proposed in which the oxygen atom of N_2O was transferred to the O^{2-} ion in a four-center NN−O−O^{2-} linear transition state. The calculations were based on an embedded cluster technique, and the energy barrier height was calculated to be 27 kcal/mol for an O^{2-} ion seated in the CaO(100) surface and 26 kcal/mol for a three-coordinated corner O^{2-} site. When compared to the 34 kcal/mol of Winter, these values were assumed to be low. The discrepancies were attributed to the computational technique used, as it underestimated the N−O bond strength in N_2O by 19 kcal/mol. In a more recent work density-functional theory and pseudopotential techniques were used to determine the energetics of N_2O dissociation on $O^{2-}_{CaO(100)}$.[10] The barrier height was 11 kcal/mol lower than the value of Winter. Again, the dissimilarity was assumed to be due to the theoretical approach used.

The activation energy for N_2O decomposition on MgO was also determined by Winter to be 35 kcal/mol in the temperature range 723−823 K, and the preexponential factor of the Arrhenius expression used was one-ninth of the factor of CaO.

* Corresponding author.

S1089-5647(98)00093-5 CCC: $15.00
Published on Web 03/13/1998

TABLE 1: Scope of Experiment

parameter	substrate		
	SiO_2	CaO	MgO
temp (K)	773−1223	773−973	773−1073
flow rate (mL/min)	972	1470−490	1864−466
res time (ms)	150	100−300	75−300
N_2O conc (ppm)	200−5000	200−5000	200−5000
O_2 conc (%)	0	0−8	0−8
surface area[a] (m^2/g)	0.0232 ± 0.0004	3.5650 ± 0.0197	50.5301 ± 0.4247
bed vol (cm^3)	5.45	5.40[b]	5.35[b]
bed voidage	0.45	0.45	0.44
cumul pore vol (cm^3/g)		0.006 74	0.257 81
porosity		0.022	0.923

[a] BET area. [b] 3 m^2 surface area.

Similar activation energies have been obtained by Angeletti et al.[11] and by Breakspere et al.,[12] namely 36 and 35.6 kcal/mol. The temperature ranges used in these works were 573−753 and 673−773 K, respectively.

The present work aims to address the dissociative reaction of N_2O on both CaO and MgO and to compare ab initio results with experimental results. To minimize the influence of stable adsorbed oxygen species, the experiments are carried out in a temperature range above the desorption temperatures of Nakamura et al. and with rather low N_2O concentrations. The ab initio activation barriers are calculated with a method different from those previously used. Thus, an independent evaluation of the previous results on CaO[9,10] is made possible. To our knowledge the dissociation of N_2O on MgO has not been studied with ab initio methods before. Therefore the results on MgO are expected to be novel.

To compare the calculated activation barriers with the experimental activation energies obtained from Arrhenius expressions, transition-state theory and collision theory are used.[13] These theories also allow a comparison between experimental and theoretical preexponential factors, which will serve as an indication of the amount of active sites in the surface.

Finally, a model of a plug-flow reactor is employed to simulate experiments performed at temperatures and N_2O concentrations similar to those used by Winter. The purpose of the simulation is to explain the difference in kinetics obtained at high and low N_2O concentrations. The following two reactions, assumed to be the key steps in N_2O decomposition on several metal oxides,[5,14] are incorporated in the model:

$$N_2O + O^{2-}_{surf} \xrightarrow{k_1} N_2 + O^{2-}_{2,surf} \qquad \text{(R1)}$$

$$O^{2-}_{2,surf} + O^{2-}_{2,surf} \xrightarrow{k_2} O_2 + 2O^{2-} \qquad \text{(R2)}$$

2. Experimental Details

The experiments were performed in a fixed-bed reactor consisting of a quartz tube (28 mm i.d. × 1000 mm) fitted with a sintered quartz frit used to support the solid particles of the fixed bed. To avoid a pressure drop in the reactor tube, the compounds examined were premixed with and supported by quartz sand. The fixed bed contained 8 g of SiO_2 (experiments without oxides) or SiO_2 mixed with an amount of each oxide to provide the desired active surface area of the catalysts and the total weight of 8 g.

The bed temperature is controlled by a thermocouple placed just over the bed. Mass-flow regulators (Brooks model 5850E) were used to set the desired gas flow that could either pass through the reactor or pass by as directed by three-way taps. The gas concentration was measured in a continuous mode at room temperature. The analyzer used was a quadrupole mass spectrometer (BALZERS QMS 311). The N_2O decomposition for the different bed materials and experimental conditions was measured by monitoring the *m*/*e* 44 signal. Table 1 shows the scope of the experimental investigation. The specific surface area and the porosity of the different bed materials were determined by using the BET method with krypton as the adsorbate. The determination was done after preheating the substance in vacuo for 3 h at 523 K. All materials examined are of analytical grade (pro analysi) and used as supplied. The experiments were performed at least twice with good reproducibility (±5%).

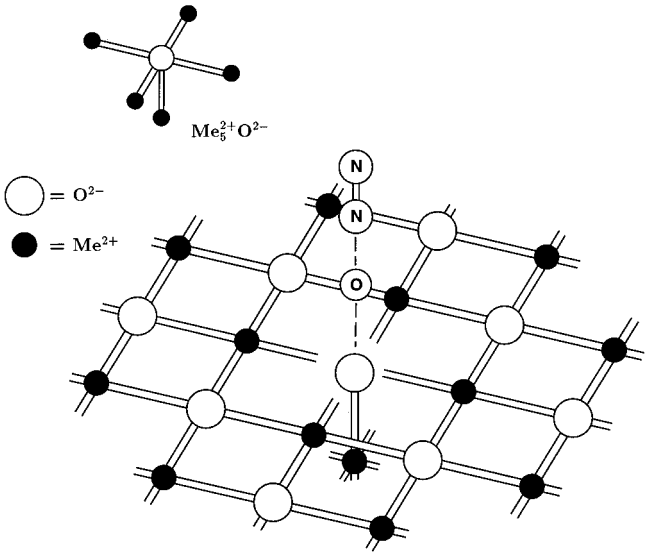

Figure 1. $Me_5^{2+}O^{2-}$ cluster used in the ab initio calculations (Me = Ca, Mg) and the N_2O dissociation on the MeO(100) model surface.

The effect of mass transport in the pores of the catalysts was measured by varying the gas residence time (75−300 ms) and the active surface area (1.5−6 m^2). The N_2O reduction for an inlet concentration of 200 ppm was unaffected when the area and the residence time were proportionally varied. This indicates that there is no internal diffusion control. All other experiments performed refer to a CaO or MgO catalyst with an area of 3 m^2.

3. Computational Details

3.1. Ab Initio. The N_2O dissociation was calculated on top of a $Me_5^{2+}O^{2-}$ cluster, which was embedded in an array of point charges placed at the lattice points (cf. Figure 1). The point charges were optimized to reproduce the Madelung potential in a volume enclosing the cluster and the reacting molecule.[15,16] Similar embedded-cluster techniques have been used in several

computational studies that address interaction between molecules and CaO or MgO surfaces. For instance, a small MgO_5 cluster surrounded by point charges was proven to be an adequate description of the MgO surface when compared to larger clusters or periodic slab calculations.[17]

The calculations were carried out with the MOLCAS-3 program package.[18] The electrons of the cluster and of the N_2O molecule were explicitly described by the atomic natural orbitals (ANO) of Pierloot et al.[19] The ANOs were 17s12p/5s4p for Ca^{2+} and 13s8p/4s3p for Mg^{2+}, respectively. The geometries of the transition states (TS) were determined at the restricted Hartree−Fock (RHF) and the second-order many-body perturbation (MP2) level of theories in C_{2v} symmetry. The ANOs of O and N were 10s6p3d/4s3p1d. Initially, the N atom nearest to the surface was held in a fixed position and the oxygen atom of N_2O was step-by-step transferred to the surface anion. For each geometry of the N and O atoms, a full RHF geometry optimization of the outer N atom and the surface O^{2-} ion was performed by employing analytical gradients. In this RHF optimized structure a MP2 calculation were carried out. The procedure was repeated with a new position of the N atom nearest to the surface until the RHF TS and the MP2 TS geometries were obtained.

To determine accurate activation barriers, a series of complete active space second-order perturbation theory (CASPT2N)[20,21] calculations around both the RHF TS and the MP2 TS geometries were performed. Only the distances of the outer N atom and the oxygen atom of N_2O were varied. The ANOs of all the oxygen and nitrogen atoms were increased to 10s6p3d/5s4p2d, and the active space in the CASSCF calculations preceding the CASPT2N calculations was large enough to include the 2p orbitals of N_2O and the $2p_\sigma$ orbital of O^{2-}. An additional occupied σ orbital was also included in order to describe the N_2-O-O^{2-} bond situation properly. Accordingly, the active space consisted of 11 orbitals and 14 electrons. Despite the fact that part of the geometry optimizations were performed with CASPT2N, the transition-state geometries are refered to as RHF TS and MP2 TS, respectively.

To estimate the effect of using an incomplete basis set, a larger basis was employed to determine the bond strength of N_2-O and $O-O^{2-}_{(100)}$. In these calculations the nitrogen and oxygen 14s9p4d3f/5s4p3d2f ANOs of Widmark et al.[22] were used.

Force-constant matrices used to determine the RHF vibrational frequencies of the transition states were computed in the C_s symmetry by a two-point finite difference formula. All the ions in the surface were kept fixed and their masses were set to infinity in the subsequent frequency analysis.

3.2. Reactor Model. The reactor was described as an ideal plug-flow reactor (PFR) operating under steady-state conditions.[23] The corresponding material balance equation for N_2O according to reaction 1 and 2 in the Introduction is

$$\frac{dN_2O(x)}{dx} = -k_1 N_2O(x)[1 - \theta(x)]\frac{C}{v} \qquad (1)$$

in which $N_2O(x)$ is the longitudinal concentration in mol/m^3, v the longitudinal plug flow in m/s, and $\theta(x)$ the longitudinal surface coverage, determined from

$$N_a k_1 N_2O(x)[1 - \theta(x)] - k_2\theta(x)^2 = 0 \qquad (2)$$

C in eq 1 is a constant equal to $\rho_{sat}A_{tot}/V_{void}$, where ρ_{sat} is the number of catalytic sites per square meter, A_{tot} the total surface area of the catalyst, and V_{void} the bed volume multiplied by the bed-voidage fraction (cf. Table 1). ρ_{sat} is set to 1.7×10^{19} and 2.4×10^{19} m^{-2} for CaO and MgO, respectively. The values correspond to surfaces in which all the oxygen anions are considered active sites and each anion occupies an area equal to the square of the lattice constant. k_1 and k_2 in eq 1 and eq 2 are the rate constants of reactions 1 and 2. They are defined by the Arrhenius expression

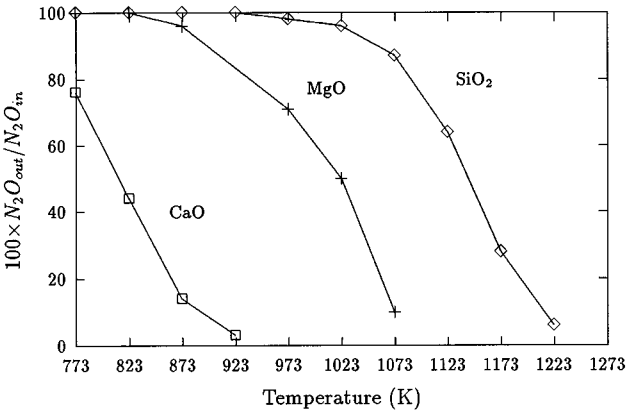

Figure 2. N_2O decomposition on CaO, MgO, and SiO_2 (N_2O_{in} = 200 ppm).

$$k_i = A_i\,(-E_{ai}/RT) \qquad (3)$$

The units of the preexponential factors A_1 and A_2 are m^3/s and s^{-1}, respectively. In this form the values of A_1 obtained from the experiments can be compared to preexponential factors calculated from collision theory and transition-state theory (ref 13 and Appendix).

The values of A_2 and E_{a2} were estimated from the TPD experiments of Nakamura et al., and they were set to 10^9 s^{-1} and 31−37 kcal/mol, respectively.

4. Results

4.1. Experiments. The background influence of the quartz reactor and the quartz sand (SiO_2) was evaluated by experiments performed without any CaO and MgO added to the fixed bed. In Figure 2 some of the results from these experiments together with results from N_2O decomposition experiments with the different oxides mixed with SiO_2 are displayed. As can be seen, the influence of SiO_2 on the N_2O decomposition on CaO is negligible, whereas the background decomposition in the temperature range of 1023−1073 K needs to be accounted for.

The catalytic activity as a function of the inlet concentration was investigated by varying the amount of N_2O between 200 and 5000 ppm. No appreciable change in the decomposition for CaO (873 K), MgO (973 K), and SiO_2 (1023 K) was obtained, and according to reaction 1 in the Introduction, the N_2O decomposition is considered to be a first-order reaction. The effect of mixing the inlet gas with O_2 was examined on both CaO and MgO. Experiments with different amounts of O_2, up to 8%, reproduced the N_2O decomposition results that were accomplished without the addition of oxygen.

The residence time dependence for an inlet N_2O concentration of 200 ppm is plotted in Figure 3. The MgO results are adjusted with regard to the background influence. Due to the low concentration, the surface coverage in eq 1 can be neglected (see section 4.4) and the preexponential factor log A_1C and the activation energy E_{a1} are obtained from the Arrhenius plots in Figure 4. The values are presented in Table 2 together with A_1.

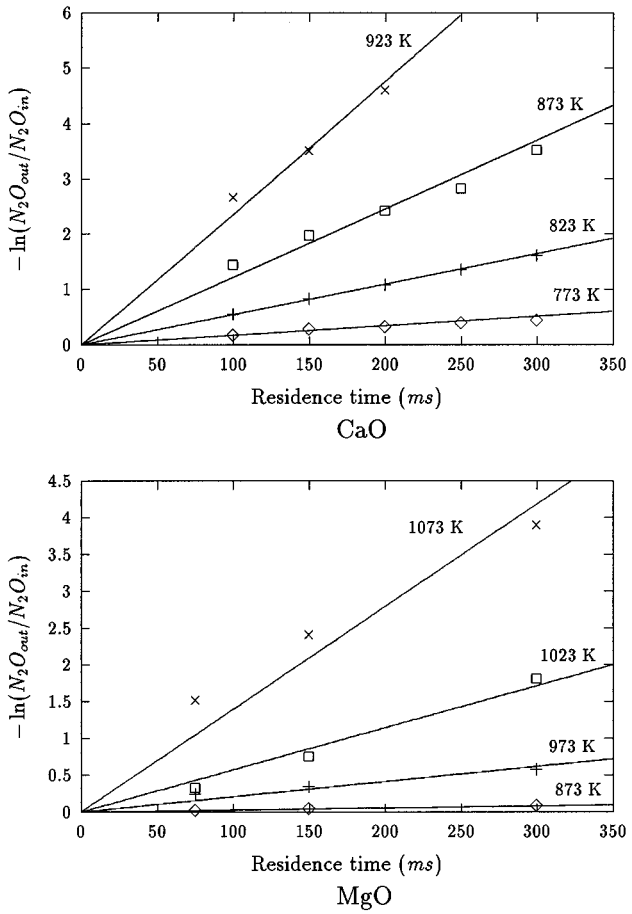

Figure 3. N_2O decomposition as a function of residence time (N_2O_{in} = 200 ppm).

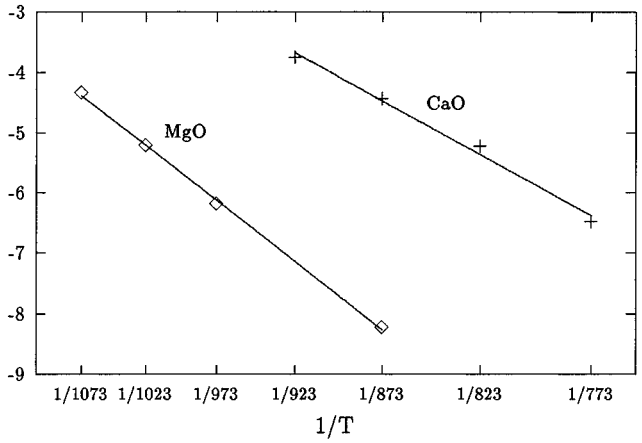

Figure 4. Arrhenius plots of the slopes in Figure 4.

TABLE 2: Experimental Activation Energies, E_{a1} (kcal/mol), and Preexponential Factors, log A_1C and A_1 (10^{-18} m^3/s), for N_2O Dissocation

substrate	E_{a1}	log A_1C	A_1
CaO	25.6−27.5[a]	17.21−18.39[a]	1.4−4.5[a]
MgO	35.5[a]−36.1	19.12[a]−19.47	6.9[a]−9.9

[a] The highest temperatures in Figure 4 are excluded.

4.2. Ab Initio Calculations. Table 3 shows the calculated geometries and the barrier heights of the transition states for N_2O dissociation (cf. Figure 1). It is notable that the N_2-O distance is more stretched on MgO than on CaO. Consequently, the highest barrier is obtained for MgO, and the difference between the two substrates is 11 kcal/mol for the MP2 TS geometries.

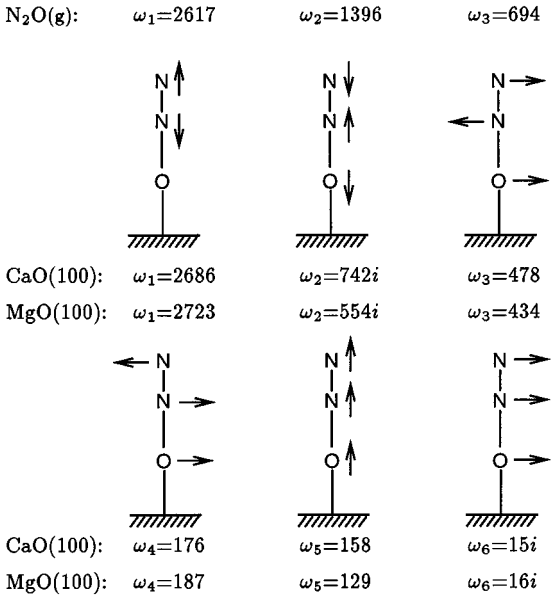

Figure 5. RHF vibrational frequencies (cm^{-1}) of N_2O(g) and the N_2-O-O^{2-} transistion state on CaO(100) and MgO(100).

TABLE 3: CASPT2N Transition-State Geometries (Å) and Activation Barriers, E_{01}[a] (kcal/mol), $N_2-O-O^{2-}_{100}$

geometry	N−N	N−O	$O-O^{2-}$	O^{2-}−(100) surf.	E_{01}
CaO(100)					
RHF TS	1.11	1.59	2.14	−0.02	24.1
MP2 TS	1.11	1.53	2.06	−0.10	22.2
MgO(100)					
RHF TS	1.11	1.69	2.14	−0.03	38.1
MP2 TS	1.11	1.61	1.99	−0.11	33.1

[a] Not corrected for zero-point energies.

TABLE 4: CASPT2N Bond Strengths[a] (kcal/mol) of $N_2-O(g)x^b$ and $O-O^{2-}_{100}$

basis set	N_2-O	$O-O^{2-}_{CaO(100)}$	$O-O^{2-}_{MgO(100)}$
5s4p2d-S	29.5	54.8	26.4
5s4p3d2f-L	41.0	59.7	32.8

[a] Corrected for zero-point energies. [b] Experiment 40 kcal/mol.[24]

From Table 4 it can be seen that the basis set used to determine the barrier heights underestimates the N−O bond strength of N_2O(g) by 11 kcal/mol, whereas the larger 5s4p3d2f basis set gives an accurate bond strength. The improvement of the surface peroxides bond strengths is somewhat lower, 5−6 kcal/mol, when the larger basis set is used. Thus, in the complete basis set limit the CASPT2N barrier heights would presumably be a few kcal/mol higher than those presented in Table 3.

The vibrational frequencies of the transition states presented in Figure 5 reveal two imaginary modes, where the first one, ω_2, corresponds to the mode that transfers the complex through the saddle point. The low value of the second imaginary frequency, ω_6, indicates that the potential energy surface for an angular movement of the entire linear complex is rather shallow. Calculations where the angle between the molecular axis and the surface was varied and the atomic distances were kept fixed demonstrated that the corresponding potential is a double well with an almost infinite depth due to the interaction between the atoms and the surface ions. By fitting a harmonic potential to the double-well potential, neglecting the small

TABLE 5: Calculated Preexponential Factors (10^{-18} m^3/s) and Activation Energies (kcal/mol) for N_2O Dissociation (cf. the Equations in the Appendix)[a]

theory	A_{TH1}	A_1	E_{01}	E_{a1}
CaO(100)				
transition state	0.61	12.2	20.5	25.5
collision	6.1	10.1	20.5	21.3
MgO(100)				
transition state	1.50	30.1	31.4	37.4
collision	6.8	11.2	31.4	32.4

[a] The temperature is 800 K for CaO and 1000 K for MgO, respectively. $\kappa = 1$ and eneriges are corrected for zero-point vibrations according to the frequencies in Figure 5.

central barrier, a frequency of approximately 20 cm^{-1} was calculated for both CaO and MgO.

4.3. Theoretical Rate Constants. The rate-determining parameters in Table 5 are calculated from the theoretical expressions presented in Appendix. The frequencies in Figure 5, except ω_6, which was replaced by 20 cm^{-1} (see above), were used to estimate the zero-point energy corrections as well as the transition-state preexponential factors (A_{TS} in eq A.2). The collision-theory preexponential factors were calculated by equating the collision diameter, σ_r in eq A.5, with the ionic radius of O^{2-} (1.4 Å[24]) plus half the length of N_2O(g) (1.16 Å[24]). The mass of the $O^{2-}_{(100)}$ ion was set equal to infinity, and θ_r in eq A.6, the angle between the *z*-axis perpendicular to the surface and the four-center molecular axis, was set equal to 25°. This angle corresponds to the point on the double-well potential where the energy is almost the same as at the central barrier.

A_1 and E_{a1} in Table 5 are the preexponential factors and the activation energies evaluated in accordance with the general definition of E_a (eqs A.8 and A.9). The values are obtained with fixed temperatures: 800 K for CaO and 1000 K for MgO, respectively. It should be remarked that the difference between these values and A_{TH1} and E_{01} results from the fact that the theoretical preexponential factors are temperature dependent. This is not the case for the preexponential factor of the Arrhenius expression used to obtain the experimental values in Table 2. However, it is reasonable to compare the experimental results in Table 2 with A_1 and E_{a1} in Table 5, since $\ln k(T)_1$ is expected to be well approximated by a linear function of $1/T$ within the rather narrow experimental temperature ranges.

4.4. Modeling. From eq 2 in section 3.2 the surface coverage at different conditions can be estimated. For instance 800 K, 200 ppm of N_2O, and the rate-determining parameters $A_1 = 1.4 \times 10^{-18}$ m^3/s, $E_{a1} = 25.6$ kcal/mol, $A_2 = 10^9$ s^{-1}, and $E_{a2} = 34$ kcal/mol give a maximum coverage of 0.04. Thus, at low N_2O concentrations the inhibition of the peroxide species on the decomposition rate is almost negligible. For high N_2O concentrations the inhibition may of course have a significant effect. If the activation barrier for oxygen desorption is higher than the N_2O dissociation barrier, the temperature dependence of the overall reaction rate may reflect the former process instead of the latter. This can be seen to occur in Table 6, where experimental conditions similar to those of Winter are modeled. For CaO the activation energies, E_a, obtained by fitting Arrhenius plots to the modeled points in Figure 6, are almost the same as the assumed desorption activation energies, E_{a2}. Furthermore, the preexponential factor, A, increases with the activation energy, and the values are higher than those of A_1. On MgO, where the activation barrier for desorption probably is lower than the N_2O dissociation barrier, the overall activation energies and preexponential factors are almost the same as E_{a1} and A_1.

TABLE 6: PFR Simulated Overall Activation Energies, E_a (kcal/mol), and Preexponential Factors log *AC* and *A*, for N_2O Decomposition on CaO (cf. Figure 6)

E_{a1}	A_1 (m^3/s)	E_{a2}	A_2 (s^{-1})	E_a	log *AC*	*A* (m^3/s)
			CaO			
25.6	1.4×10^{-18}	31	10^9	28.4	18.74	6.4×10^{-18}
25.6	1.4×10^{-18}	34	10^9	33.3	21.28	8.2×10^{-17}
25.6	1.4×10^{-18}	37	10^9	36.9	21.98	1.6×10^{-16}
			MgO			
36.1	9.9×10^{-18}	28	10^9	36.1	19.09	6.4×10^{-18}
36.1	9.9×10^{-18}	31	10^9	36.0	19.04	6.1×10^{-18}
36.1	9.9×10^{-18}	34	10^9	36.0	18.95	5.6×10^{-18}

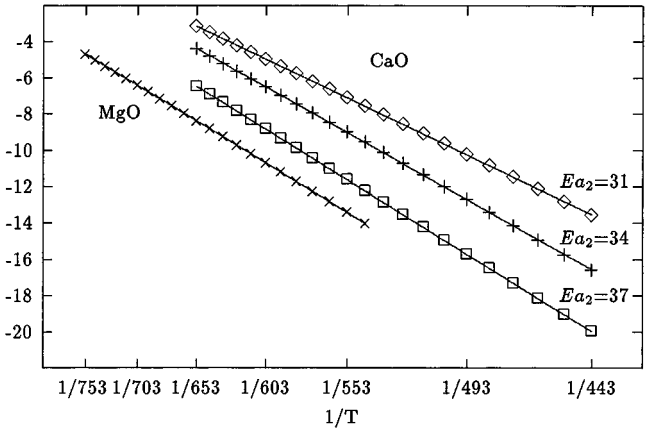

Figure 6. Simulated Arrhenius plots of a PFR working under steady-state conditions. The N_2O inlet concentration was set to 20%, and the residence time was 0−20 s. The rate-determining coefficients used in the model are displayed in Table 5 together with the overall activation energies and preexponential factors obtained from the slopes.

5. Discussion

The experimental data in Table 2 and the calculated values in Table 5 show that the activation energy for N_2O dissociation is approximately 10 kcal/mol lower on CaO than on MgO. This is a result of the difference in Madelung potential. Due to the weaker field, the O^{2-} ions in CaO(100) are more disposed to use their charge in chemical bonds. Thus, the N−O bond of N_2O does not have to be as stretched as on MgO before the $2p_\sigma$ orbital of the O atom, and the doubly occupied $2p_\sigma$ orbital of the O^{2-} ion will form a peroxide bond. Accordingly, a shorter N−O bond distance is obtained at the transition state, and the activation barrier is lowest for CaO.

It is notable that both experiments and calculations predict the preexponential factor to be highest for MgO. However, the transition-state values seem to be somewhat high when compared to experiments. Lower values, for instance setting $\kappa < 1$ in eq A.2, will lead to lower E_{a1} values. This is not so critical since the E_{01} values are assumed to be a few kcal/mol too low due to the incomplete basis set used (see section 4.2).

The difference in activation energy between the two substrates and the values of the preexponential factors contradict the overall kinetic results of Winter, who obtained similar activation energies and a preexponential factor for CaO that was higher than the one for MgO. The discrepancies are explained by the modeling results, which are more in accordance with the results of Winter. Thus, at high N_2O concentrations the overall activation energy for CaO is close to the activation energy of the desorption process, and the increase in activation barrier is accompanied by an increase of the overall preexponential factor.

The rather good agreement between the experimental and the calculated data indicates that the five-coordinated oxygen ions in both CaO(100) and MgO(100) participate in the dissociative

process. Moreover, on these sites it seems as oxygen is not able to dissociate, since the decomposition rate did not change when oxygen was present in the inlet gas. This is also emphasized by Nakamura et al., who established that no oxygen desorbed from a CaO surface that had been preexposed to molecular oxygen.

The appeared resistance toward oxygen dissociation is explained in ref 25, and it is understood from the electronic structures of the peroxides. These species are singlets in their ground states. Thus, an associative reaction between two oxygen atoms adsorbed as peroxides implies that the atoms leave the ionic CaO surface as a molecule with paired electrons. Once the oxygen has left the surface, the molecule is likely to be quenched into its triplet ground state. Consequently, a readsorption is expected to be an improbable process.

6. Concluding Remarks

A comparative analysis of N_2O dissociation on CaO and MgO is provided in the present effort. Both experiments and ab initio calculations predict the CaO surface to be the most active catalyst. The experimental activation energies are 26 kcal/mol for CaO and 36 kcal/mol for MgO, respectively. When compared with these values, the calculated activation energies differ by 0−5 kcal/mol depending on the values used for the theoretical preexponential factors. It is suggested that most of the anionic sites in the CaO and MgO substrates are active in dissociating N_2O at the temperatures investigated, since a good agreement between calculated and experimental activation energies and preexponential factors is obtained.

The PFR model demonstrates that the value of 34 kcal/mol for the overall decomposition rate on CaO obtained by Winter[6] reflects the activation energy toward oxygen desorption and not the N_2O dissociation. In the same work the preexponential factor of the Arrhenius expression used to describe the overall decomposition was higher for CaO than for MgO. This is opposite the result obtained with low N_2O concentrations. The model shows that at high N_2O concentrations a change in order of the overall preexponential factor could be expected when the activation energy toward oxygen desorption becomes higher than the N_2O dissociation barrier.

Finally, it is concluded that the catalytic activity of the lattice oxygen anions of CaO and MgO follows the trend MgO < CaO < SrO < BaO and that most of these anions are resistant toward oxygen dissociation. Thus, anions in several metal oxides may contribute significantly to the decomposition of N_2O at high temperatures.

Acknowledgment. The Swedish National Board for Industrial and Technical Development and the Swedish Research Council for Engineering Science are gratefully acknowledged for their financial support.

Appendix

The transition-state theory rate constant is

$$k_{TS} = A_{TS} \exp(-E_0/RT) \tag{A.1}$$

where E_0 is the energy barrier corrected for the zero-point energies. Assuming that the contribution from the surface ions in the reaction

$$N_2O + O^{2-}_{100} \rightleftharpoons N_2O{-}O^{2-\ddagger}_{100} \rightarrow N_2 + O^{2-}_{2,100}$$

are negligible, the preexponential factor A_{TS} is

$$A_{TS} = \kappa \frac{kT}{h} \frac{q_{N_2O-O^{2-\ddagger}_{100}}}{q_{N_2O}} \tag{A.2}$$

κ is the transmission coefficient and q_{N_2O} is the molecular partition function for N_2O(g) including the translational, vibrational, and rotational degrees of freedom:

$$q_{N_2O} = q_t q_{\omega_1} q_{\omega_2} q_{\omega_3}{}^2 q_r \tag{A.3}$$

For the activated complex vibrational degrees of freedom only contribute (cf. Figure 5), and the partition function is

$$q_{N_2O-O^{2-\ddagger}_{100}} = q_{\omega_1} q_{\omega_3}{}^2 q_{\omega_4}{}^2 q_{\omega_5} q_{\omega_6}{}^2 \tag{A.4}$$

The collision-theory preexponential factor for a bimolecular reaction is

$$A_{CT} = \left(\frac{8kT\tau}{\mu}\right)^{1/2} \sigma_R{}^2 P \tag{A.5}$$

where μ is the reduced mass, σ_r is the hard-sphere collision diameter, and P is the steric factor. For a reaction similar to $N_2O + O^{2-}_{100}$ a simple estimation of P is the reactive solid angle divided by $2\times 2\pi$, i.e.,

$$P = \frac{1}{2}\int_0^{\theta_r} \sin\theta \, d\theta \tag{A.6}$$

θ is the angle between the z -axis perpendicular to the surface and the four-center molecular axis.

Experimental data obtained from the Arrhenius law can be compared to the above theoretical (TH) values via the general definition of activation energy:

$$E_a = RT^2 \frac{\partial \ln k}{\partial T} \tag{A.7}$$

Thus,

$$E_a = E_0 + RT^2 \frac{\partial \ln A_{TH}}{\partial T} \tag{A.8}$$

and the preexponential factor is

$$A = \exp\left(T \frac{\partial \ln A_{TH}}{\partial T}\right) A_{TH} \tag{A.9}$$

References and Notes

(1) Pacchioni, G.; Ricart, J. M.; Illas, I. *J. Am. Chem. Soc.* **1994**, *116*, 10152−10158.
(2) Nygren, M. A.; Pettersson, L. G. M. *Chem. Phys. Lett.* **1994**, *230*, 456−462.
(3) Miettinen, H.; Strömberg, D.; Lindqvist, O. *11th international conference on fluidized bed combustion*; Anthony, E. J., Ed.; Canmet, 1991; Vol. 2, pp 999−1003.
(4) Winter, E. R. S. *J. Catal.* **1970**, *19*, 32−40.
(5) Nakamura, M.; Mitsuhashi, H.; Takezawa, N. *J. Catal.* **1992**, *138*, 686−693.
(6) Snis, A.; Panas, I.; Strömberg, D. *Surf. Sci.* **1994**, *310*, L579−L582.
(7) de Soete, G. G. Combustion related heterogeneous reactions involving N_2O. *Proceedings of the Fifth International Workshop on Nitrous Oxide Emissions*, NIRE/IFP/EPA/SCEJ, Tsukuba, Japan, 1992, pp 199−222.
(8) Pels, J. R. Nitrous oxide in coal combustion, Ph. D. Thesis, Technische Universiteit Delft, ISBN 90-5166-466-X, Eburon, Delft, 1995.
(9) Snis, A.; Strömberg, D.; Panas, I. *Surf. Sci.* **1993**, *292*, 317−324.
(10) Kantorovich, L. N.; Gillan, M. J. *Surf. Sci.* **1997**, *376*, 169−176.
(11) Angeletti, C.; Cimino, A.; Indovina, V.; Pepe, F.; Schiavello, M. *Z. Phys. Chem. (Wiesbaden)* **1980**, *122* (2), 237−249.

(12) Breakspere, R. J.; Hassan, L. A. R.; Roberts, D. K. *J. Chem. Soc., Faraday. Trans. 1* **1975**, *71*, 2251.

(13) Smith, I. W.M. *Kinetics and dynamics of elementary gas reactions*; ISBN 0-408-70790-9; Butterworth and Co Ltd.: London, 1980.

(14) Vijh, A. K. *J. Catal.* **1973**, *31*, 51−54.

(15) Børve K.; Pettersson, L. G. M. *J. Phys. Chem.* **1991**, *95*, 7401.

(16) Parry, D. E. *Surf. Sci.* **1975**, *49*, 433; Errata *Surf. Sci.* **1976**, *54*, 195.

(17) Pacchioni, G,; Neyman, K.; Rosch, N. *J. Electron Spectrosc. Relat. Phenom.* **1994**, *69*, 13.

(18) Andersson, K.; Fülscher, M. P.; Karlström, G.; Lindh, R.; Malmqvist, P. Å.; Olsen, J.; Roos, B. O.; Sadlej, A. J.; Blomberg, M. R. A.; Siegbahn, P. E. M.; Kellö, V.; Noga, J.; Urban, M.; Widmark, P. O., *MOLCAS* Version 3; Dept. of Theor. Chem., Chem. Center, Univ. Of Lund, P.O.B. 124, S-221 00 Lund, Sweden, 1994.

(19) Pierloot, K.; Dumez, B.; Roos, B. O. *Theor. Chim. Acta* **1995**, *90*, 87.

(20) Andersson, K.; Malmqvist, P. Å.; Roos, B. O.; Sadlej, A. J.; Wolinski, K. *J. Phys. Chem.* **1990**, *94*, 5483.

(21) Andersson, K.; Malmqvist, P. Å.; Roos, B. O. *J. Chem. Phys.* **1992**, *96*, 1218.

(22) Widmark, P. O.; Malmqvist, P. Å.; Roos, B. O. *Theor. Chim. Acta* **1990**, *77*, 291.

(23) Dumesic, J. A.; Rudd, D. F.; Aparicio, L. M.; Rekoske, J. E.; Trevino, A. A. *The Microkinetics of Heterogeneous Catalysis*; ACS Professional Reference Book, ISBN 0-8412-2214-2; Washington, DC, 1993.

(24) *Handbook of Chemistry and Physics*, 60th ed.; Weast, R. C., Ed.; CRC Press: Cleveland, 1979.

(25) Snis, A.; Panas, I. *J. Chem. Phys.* **1995**, *103*, 7626.